

Optical Properties of the Products of α -Dicarbonyl and Amine Reactions in Simulated Cloud Droplets

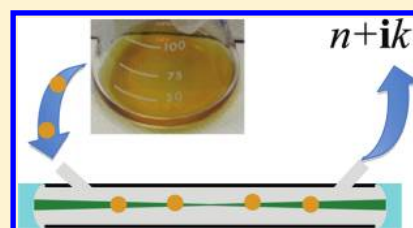
Kyle J. Zarzana,^{†,‡} David O. De Haan,^{‡,§} Miriam A. Freedman,^{‡,||} Christa A. Hasenkopf,^{‡,⊥} and Margaret A. Tolbert^{†,‡,*}

[†]Department of Chemistry and Biochemistry and [‡]Cooperative Institute for Research in Environmental Sciences (CIRES),

[⊥]Department of Atmospheric and Oceanic Sciences, University of Colorado at Boulder, Boulder, Colorado 80309-0216, United States

[§]Department of Chemistry and Biochemistry, University of San Diego, 5998 Alcalá Park, San Diego, California, 92110

ABSTRACT: Secondary organic aerosol makes up a significant fraction of the total aerosol mass, and a growing body of evidence indicates that reactions in the atmospheric aqueous phase are important contributors to aerosol formation and can help explain observations that cannot be accounted for using traditional gas-phase chemistry. In particular, aqueous phase reactions between small organic molecules have been proposed as a source of light absorbing compounds that have been observed in numerous locations. Past work has established that reactions between α -dicarbonyls and amines in evaporating water droplets produces particle-phase products that are brown in color. In the present study, the complex refractive indices of model secondary organic aerosol formed by aqueous phase reactions between the α -dicarbonyls glyoxal and methylglyoxal and the primary amines glycine and methylamine have been determined. The reaction products exhibit significant absorption in the visible, and refractive indices are similar to those for light absorbing species isolated from urban aerosol. However, the optical properties are different from the values used in models for secondary organic aerosol, which typically assume little to no absorption of visible light. As a result, the climatic cooling effect of such aerosols in models may be overestimated.



INTRODUCTION

Atmospheric aerosol particles play a significant but poorly understood role in affecting the Earth's radiative balance. Aerosol particles can directly interact with light by scattering or absorbing incoming radiation, and the amount of scattering or absorption determines whether aerosol particles have a net warming or cooling effect on climate.^{1,2} The amount of light that a substance scatters versus absorbs can be quantified by the complex refractive index

$$m = n + ik \quad (1)$$

where n , the real part, describes the scattering, whereas k , the imaginary part, describes the absorption. The complex refractive index of aerosol particles is a useful quantity to measure because unlike other means of quantifying scattering and absorption, such as the single scatter albedo, the refractive index depends primarily on composition and does not depend on particle size or concentration. Using the refractive index and the particle shape, secondary quantities such as the absorption and scattering cross sections and the single scatter albedo can be calculated.

Globally, organic compounds make up 50% of aerosol mass, and in polluted areas this amount can be as high as 90%.³ Given the ubiquity and dominance of organic aerosol (OA), understanding the optical properties of OA is crucial to predicting its effects on radiative forcing. The traditional formation mechanism of OA is through the gas phase oxidation of volatile organic compounds (VOCs), which then condense

to form aerosol. The compounds that are formed by this route are typically assumed in models to be non or only slightly absorbing in the visible; that is they have a k value close or equal to zero.^{4–6} However, there is growing evidence that a substantial amount of OA does absorb in the visible, particularly at shorter wavelengths. These compounds have been termed “brown carbon”⁷ and have been observed in both urban^{8–10} and rural^{10–12} environments. Recent reviews have pointed to the role that aqueous chemistry can play in increasing aerosol mass^{13,14} and the products of many of these reactions, including reactions on acidic particles,¹⁵ aldol condensation reactions,¹⁶ and reactions with various nitrogen-containing species,¹⁷ produce species that absorb visible light, in addition to numerous nonabsorbing compounds.

Much of the work on aqueous aerosol chemistry has focused on the role of glyoxal and methylglyoxal. Glyoxal and methylglyoxal are the smallest α -dicarbonyls and due to their high volatility cannot condense into the organic phase of particles through traditional gas-particle partitioning. However, both readily partition to the aqueous phase and have been shown to react with a number of species to form light-absorbing compounds.^{18–20} De Haan et al.^{21–23} have shown that glyoxal and methylglyoxal can undergo aqueous phase

Received: November 10, 2011

Revised: March 21, 2012

Accepted: April 9, 2012

Published: April 19, 2012

reactions with primary amines, producing a variety of compounds including oligomers and imidazoles. These compounds contain carbon–nitrogen bonds, a feature commonly observed in ambient aerosol.^{24,25} Additionally, the product mixtures are brown in color, and therefore contribute to light absorption in the visible.

The present study builds on previous work that examined the formation kinetics and aerosol products of aqueous phase reactions.^{21–23} The goal of the present study is to quantify the optical properties of model secondary organic aerosol formed by these aqueous phase reactions. The refractive indices of compounds from four model systems were determined and then compared to field measurements of brown carbon aerosol. Using the calculated refractive indices, the single scattering albedo and the relative forcing in the visible of the particles were also calculated. Additionally, estimates of the cooling effect of these particles and particles used in climate models are presented.

EXPERIMENTAL SECTION

Four model systems were studied: glyoxal-glycine; glyoxal-methylamine; methylglyoxal-glycine; and methylglyoxal-methylamine. Solid glyoxal trimer dihydrate, solid glycine, 40% w/w aqueous methylamine (all Sigma Aldrich), and 40% w/w aqueous methylglyoxal (MP Biomedicals) were used without further purification. Samples were generated in a manner similar to the bulk phase samples used by De Haan et al.^{21–23} One M stock solutions of each were created, and then 150 μL of an α -dicarbonyl (either glyoxal or methylglyoxal) was combined with 150 μL of an amine (either glycine or methylamine) in small vials and allowed to dry for several days at room temperature. These concentrations were chosen in order to be consistent with the concentrations used by De Haan et al.,^{21–23} and we note that while the concentrations of dicarbonyls and amines vary depending on location, these compounds can exist at roughly equal concentrations, particularly in urban areas.^{26,27} Additionally, while this reaction time is longer than the lifetime of an atmospheric cloud droplet, the rate of these reactions is significantly increased by the drying process, and analysis of mass spectrometer data of products from both bulk reactions and simulated cloud droplet reactions indicate that the products are chemically similar.^{21,22} The resulting brown product was then dissolved in HPLC-grade water, and atomized (TSI 3076) using prepurified nitrogen. The aerosol was passed through two custom-made 4 L Erlenmeyer flask driers and two diffusion driers (TSI model 3062) to remove the water and reduce the relative humidity (RH) to <10%.

The aerosol particles were analyzed using an atomic force microscope (AFM) to determine their morphology. The dry, polydisperse aerosol particles were collected for several hours on $\text{SiO}_x/\text{Si}(100)$ wafers. The aerosol samples were analyzed at ambient RH ($\sim 30\%$) with a Veeco Dimension 3100 AFM equipped with a Nanoscope IVa controller. The instrument was used in tapping mode with silicon tips (Nanosensors PPP-FMR, spring constant = $2.5\text{--}4\text{ N m}^{-1}$).

A cavity ring-down aerosol extinction spectrometer (CRD) was used to determine the refractive indices of the particles. The CRD is shown schematically in Figure 1. This instrument has been described elsewhere^{28,29} and so only a brief summary is provided here. The second harmonic of a Nd:YAG laser (Quantel USA) is used to generate 532 nm light, which is then coupled into a cavity capped with two highly reflective mirrors

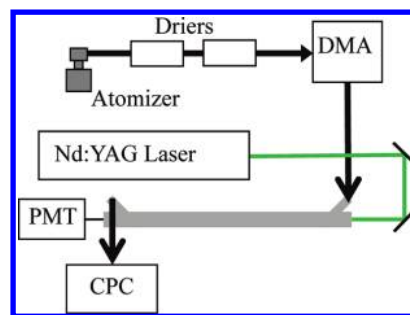


Figure 1. Setup for cavity ring-down experiments. Four driers were used in the experiments, but only the two diffusion driers are shown for simplicity.

($R > 99.998\%$, Advanced Thin Films). The light that enters the cavity reflects off the mirrors numerous times, and the time decay of the signal that is transmitted out the other end is measured with a photomultiplier tube (PMT, Hamamatsu HC120). The decay time is measured under conditions when there is no aerosol present in the cavity (τ_0) and when the aerosol is present (τ). The extinction, α_{ext} (with dimensions of inverse length) is then calculated from

$$\alpha_{\text{ext}}(\text{Mm}^{-1}) = \frac{R_L}{c} \left(\frac{1}{\tau} - \frac{1}{\tau_0} \right) \quad (2)$$

where c is the speed of light and R_L is the ratio of whole cavity length to the length that the aerosol sample occupies. For this system, the ring-down time for the aerosol-free cavity, τ_0 , is approximately 100 μs , which corresponds to an effective path length of $\sim 30\text{ km}$.

To determine the refractive index, the dried polydisperse aerosol first enters a differential mobility analyzer (DMA, TSI model 3081), which allows through only particles of a single electrical mobility diameter. The monodisperse flow enters the CRD, where the extinction is determined. The aerosol concentration is then measured with a condensation particle counter (CPC, TSI model 3022 and 3775). This process is repeated for a range of diameters between 200 and 500 nm, so that at each diameter the extinction and concentration are determined. The extinction measured by the CRD depends on both the particle size and concentration

$$\alpha_{\text{ext}} = \frac{CQ_{\text{ext}}(n, k, D, \lambda)\pi D^2}{4} \quad (3)$$

where C is the number concentration, Q_{ext} is the dimensionless extinction efficiency, and D is the particle diameter. Q_{ext} is a function of the particle diameter, the wavelength of incident light, λ , and the real and imaginary parts of the refractive index. The refractive index does not vary with particle size, and by stepping through different particle sizes and concentrations, the refractive index can be calculated.

The DMA size-selects by applying a uniform charge distribution to the particles and then selecting for particles based on electrical mobility. For singly charged spherical particles, the electrical mobility diameter is equal to the physical diameter of the particle regardless of the particle's density.³⁰ However, a small but non-negligible fraction of the particles exiting the DMA will have multiple charges and a physical diameter that is significantly greater than the mobility diameter. Past experience has shown that although the concentrations of particles with three or more charges is negligible, the

concentration of doubly charged particles is significant and must be accounted for when determining the refractive index. In order to reduce the number of doubly charged particles, all measurements began at a diameter at least 75 nm greater than the mode diameter of the aerosol distribution from the atomizer. This limited the fraction of doubly charged particles to less than 0.1. Additionally, because the relative amounts of particles receiving one charge versus two charges is known for each diameter,³¹ the fraction of doubly charged particles can be calculated at each size, and the contribution of the doubly charged particles to the total extinction can be determined. Previous work has verified that the method used to calculate the concentration of doubly charged particles is accurate to within 5%.²⁹

The extinction measured at each diameter is the sum of the extinction from singly charged particles and the larger doubly charged particles.

$$\alpha_{\text{ext(theory)}} = \frac{C_{+1}Q_{\text{ext},+1}(n, k, D_{+1}, \lambda)\pi D_{+1}^2}{4} + \frac{C_{+2}Q_{\text{ext},+2}(n, k, D_{+2}, \lambda)\pi D_{+2}^2}{4} \quad (4)$$

The diameters of the singly and doubly charged particles are known, and the concentration of each can be calculated using the experimentally measured total concentration. The extinction efficiency at each size can be calculated for a given value of n and k using a Mie code written in MATLAB for spherical particles,³² based on the Fortran code from Bohren and Huffman.³³ The calculated extinction value is determined by summing the extinction from both the doubly and singly charged particles for a given index of refractive. The calculated total extinction is then compared to the measured extinction. The best-fit refractive index is determined by minimizing the reduced cumulative fractional difference (CFD_r).

$$\text{CFD}_r = \frac{1}{N} \sum_{i=1}^N \frac{|\alpha_{\text{ext(theory)}} - \alpha_{\text{ext(measured)}}|}{\alpha_{\text{ext(measured)}}} \quad (5)$$

where N is the number of diameters used, $\alpha_{\text{ext(theory)}}$ is the calculated extinction, and $\alpha_{\text{ext(measured)}}$ is the measured extinction. The CFD_r is calculated for a wide range of n and k values, and the value of n and k that gives the lowest CFD_r is taken to be the refractive index for the compound. Our method for accounting for the contribution of doubly charged particles and retrieving the refractive index has been validated for both nonabsorbing and absorbing compounds.^{28,29}

RESULTS AND DISCUSSION

AFM Analysis. If the particles are spherical, the mobility diameter reported by the DMA is equal to the physical diameter,³⁰ and our use of Mie codes for spherical particles is appropriate. Representative AFM images for the four systems studied are shown in Figure 2. In nearly all cases the particles observed were spherical, justifying our assumption of sphericity in the calculations. In a few instances, large aggregates of spherical particles were observed, as shown in Figure 2d. This aggregation could have occurred during the course of collecting the particles on the silicon wafers. In all cases the nonspherical aggregates were larger than 500 nm and would be removed by the DMA and not used in our analysis.

CRD Analysis. The extinction and concentration of the particles were measured at particle diameters ranging from 200

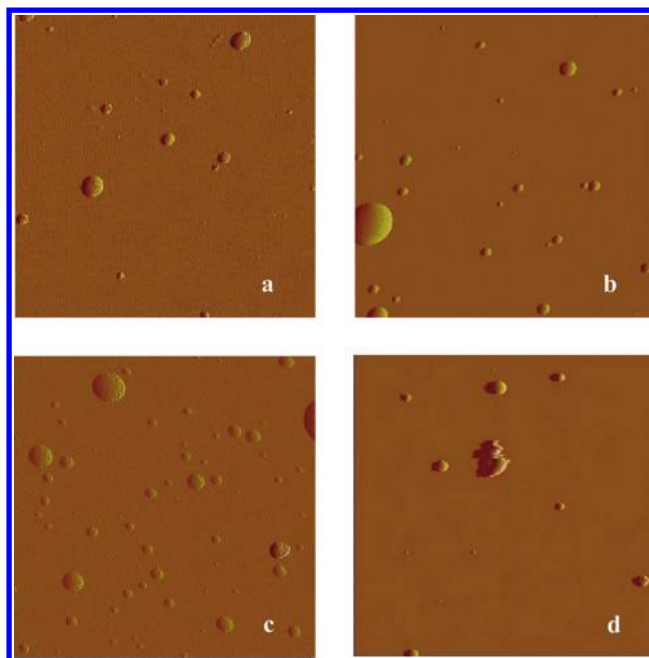


Figure 2. Sample AFM images of (a) glyoxal-glycine, (b) glyoxal-methylamine, (c) methylglyoxal-glycine, and (d) methylglyoxal-methylamine. The particles were collected on silicon wafers. All images are $5 \times 5 \mu\text{m}$.

nm to either 450 or 500 nm. While a significant number of particles exist at diameters below 200 nm, these particle sizes were not used due to the large number of doubly charged particles present at those sizes. Since the refractive index does not depend on particle size, no error is introduced by our choice of particle size range. The fraction of doubly charged particles present at each diameter was determined, and then the refractive index was calculated as described above. All CFD_r values were less than 0.05, which indicates that the retrieved n and k values provided a fit that agreed with the measured data to within 5%. A sample contour plot of the CFD_r plotted versus n and k for the glyoxal-glycine system is shown in Figure 3a, with the hotter colors corresponding to lower (better fitting) CFD_r values. The lowest CFD_r value, corresponding to the best-fit refractive index, occurs at $m = 1.62 + 0.035i$. The best-fit refractive index was used to calculate the extinction efficiency as a function of size to verify that all diameters are fit equally well. Figure 3b shows the measured and calculated extinction efficiencies as a function of diameter. The measured values have been corrected for doubly charged particles, and there is good agreement at all sizes between the measured and calculated values.

The calculated refractive index values are listed in Table 1. It should be noted that these values are for the entire mixture of products. Determining the refractive index of a mixture based on the refractive indices of the individual components can potentially lead to large errors, especially when absorbing compounds are present.^{28,34} Since the reactions lead to a mixture of products, we have determined the refractive index of the mixture. Additionally, different starting concentrations and atmospheric conditions could change the final optical properties, and these effects will need to be explored in future work.

For each system, at least five individual experiments were performed, and the refractive index was fit separately for each experiment. The reported values and error bars are the averages

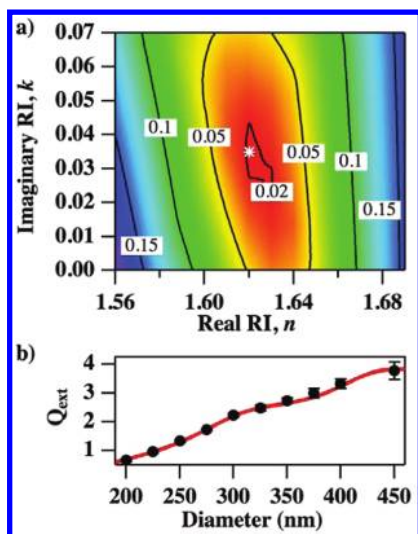


Figure 3. (a) Sample contour plot showing CFD_r plotted versus n and k for glyoxal-glycine. The hotter colors indicate a lower CFD_r value, corresponding to a better fit. The minimum CFD_r is at $n = 1.62$ and $k = 0.035$ and is marked with a white asterisk. (b) Plot of the measured Q_{ext} values (black marks) and the Q_{ext} values calculated (red line) using the best fit refractive index from 3a.

Table 1. Refractive Index Values Retrieved for the Systems Used in This Study, Values for Atmospheric HULIS Measured by Dinar et al.¹⁰ and Hoffer et al.,¹¹ and Values for Organic Aerosol Used in Models. All values are for $\lambda = 532$ nm

system	n	k	study
Experimental Values			
glyoxal-glycine	1.64 ± 0.02	0.044 ± 0.017	this study
glyoxal-methylamine	1.65 ± 0.02	0.035 ± 0.017	this study
methylglyoxal-glycine	1.64 ± 0.01	0.037 ± 0.007	this study
methylglyoxal-methylamine	1.55 ± 0.04	0.114 ± 0.037	this study
pollution HULIS	1.595 ± 0.004	0.049 ± 0.006	Dinar et al. 2008 ¹⁰
smoke HULIS	1.622 ± 0.003	0.048 ± 0.009	Dinar et al. 2008 ¹⁰
K-pusztá HULIS	1.561 ± 0.002	0.003 ± 0.004	Dinar et al. 2008 ¹⁰
HULIS- day	1.653	0.0019	Hoffer et al. 2006 ¹¹
HULIS- night	1.685	0.0016	Hoffer et al. 2006 ¹¹
Model Values			
organic carbon (same as AS)	1.529	1×10^{-7}	Myhre et al. 2007 ⁵
organic carbon	1.53	0.006	Kinne et al. 2003 ⁶

and standard deviations from the individual fits for each system. The values for all systems except methylglyoxal-methylamine are similar, with the difference between the values for each system being less than the uncertainty within each system. The refractive index for the methylglyoxal-methylamine system has a k value that is significantly higher than the values of the other three systems. Reactions of methylglyoxal have been observed to form light-absorbing material more rapidly than analogous glyoxal reactions.^{18,19} Furthermore, the production of light-absorbing material in glyoxal – amino acid reactions increases as a function of pH,³⁵ and the methylamine reaction mixtures

would be expected to have higher pH values than the glycine mixtures. Thus it is not surprising that the methylglyoxal-methylamine reaction products had the highest k value.

The refractive index values that we report have a significantly greater absorption and scattering components than the values typically used in models (Table 1). Given the complexity of organic aerosol, there are few measurements of the optical constants for light absorbing species found in ambient aerosol particles. However, two studies have examined the optical properties of humic-like substances (HULIS) extracted from ambient particles. The HULIS extract contains high molecular weight species that in some regions can make up 15–60% of the water-soluble organic compounds found in aerosol particles, and unlike many organic species in aerosol, HULIS have been shown to absorb in the visible.³⁶ Hoffer et al.¹¹ collected aerosols in the Amazon basin during both the day and the night, while Dinar et al.¹⁰ collected aerosol samples from two urban samples from Israel (“Smoke” and “Pollution”) and one rural site in Hungary (“K-pusztá”). In both studies, the water-soluble fraction of the aerosol samples were extracted and acidified, and the HULIS fraction was then obtained by chromatography. The HULIS samples were then atomized to generate aerosol for analysis. Hoffer et al.¹¹ determined the refractive index of the particles using a combination of nephelometer and photoacoustic spectrometer measurements, while Dinar et al.¹⁰ used a CRD system similar to the one used in the present work. In both studies, the refractive indices were determined at a wavelength of 532 nm. The values from both studies are shown in Table 1. The k values for the three rural samples (HULIS-day, HULIS-night, and K-pusztá) are roughly an order of magnitude lower than the values from our systems, while the values for the two urban samples are similar to those that we have obtained. However, the precursor compounds, glyoxal, methylglyoxal, methylamine, and glycine, have all been detected in high concentrations in urban areas,^{26,27} and based on this we believe that our results will be more applicable to evaluating the optical properties in these areas. While the sources of HULIS are not known, the comparison with the (albeit limited) field data indicates that while our values are different from those used in models, they are reasonable for at least some classes of atmospheric organic compounds.

Implications. The single scattering albedo (SSA) is a unitless value that quantifies the fraction of light that is scattered and the fraction that is absorbed. It is given by

$$SSA = \varpi = \frac{\sigma_{sca}}{\sigma_{sca} + \sigma_{abs}} \quad (6)$$

where σ_{sca} is the scattering cross section and σ_{abs} is the absorption cross section. Using Mie theory and the average refractive index, the SSA for each system was calculated as a function of size, as shown in Figure 4. All four systems have non-negligible absorption, particularly at smaller sizes. Methylglyoxal-methylamine absorbs at least 35% of incoming light, whereas the others absorb at least 15%. As was previously stated, OA is typically modeled as a purely scattering compound, which means that σ_{abs} is taken to be zero and the SSA is equal to 1 over the entire size range.

A particle that both scatters and absorbs light will affect radiative forcing differently than a purely scattering particle. To compare the effects on direct forcing of our particles with the effects of particles used in models, a modified version of the equation from Chylek and Wong² is used. This gives the change in forcing due to the presence of an aerosol layer, ΔF_{rel} ,

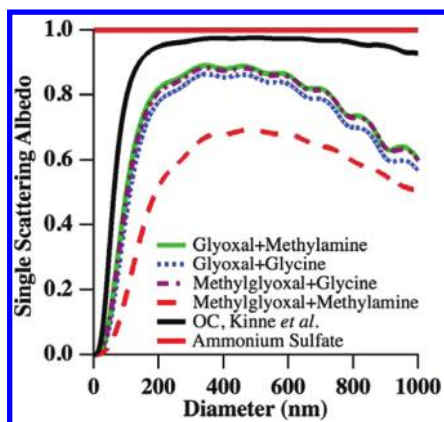


Figure 4. Single scatter albedos for all four systems and two model values plotted as a function of diameter. A single scatter albedo of 1 corresponds to a nonabsorbing compound.

$$\Delta F_{\text{rel}} = -[(1 - a)^2 \beta Q_{\text{sca}} - 2aQ_{\text{abs}}] \quad (7)$$

where a is surface albedo, Q_{sca} is the scattering efficiency, Q_{abs} is the absorption efficiency, and β is the fraction of light scattered in the upward direction. The quantity β is approximated as

$$\beta = (1 - g/2)/2 \quad (8)$$

where g is the asymmetry parameter.² The albedo, a , is set to 0.15, which is typical for urban areas.¹⁰ The scattering and absorption efficiencies and the asymmetry parameter are calculated using the refractive index of the particles and Mie theory. For the refractive indices of the systems studied here, the asymmetry parameter does not change significantly for the different systems, and the differences in relative forcing are due primarily to differences in the amount of light scattered and absorbed.

We have chosen to calculate relative forcing (ΔF_{rel}) to compare the direct effect as a function of size for our particles and for particles used in climate models. Relative forcing is a unitless quantity, and in order to calculate absolute forcing values in W/m^2 , the number distribution of the particles (the concentration at each size) must be taken into account, and additional constants, such as the fraction of sky covered by clouds, must be known. To the best of our knowledge, number distributions for brown carbon are not known or at best incompletely measured, and would be expected to vary from location to location, so for simplicity and general applicability we do not include them in our calculations. While we measure size distributions in the course of an experiment, the distributions we obtain are affected by the concentration of the solution being atomized and the flow rate used, and are not representative of ambient distributions. Additionally, the amount of cloud cover and other constants are not well constrained and can vary significantly from place to place. However, under “same sky” conditions, these numbers will be the same regardless of the optical properties of the aerosols, and so are not necessary for a relative comparison.

The ΔF_{rel} term for all four systems studied here is plotted (in arbitrary units) as a function of particle diameter in Figure 5. Additionally, the forcing terms are calculated for organic aerosol using the refractive index from the Oslo Chemical Transport Model, which treats organic compounds as non-absorbing,⁵ and the refractive index used by several other models including GOCART and GISS, which assumes a small

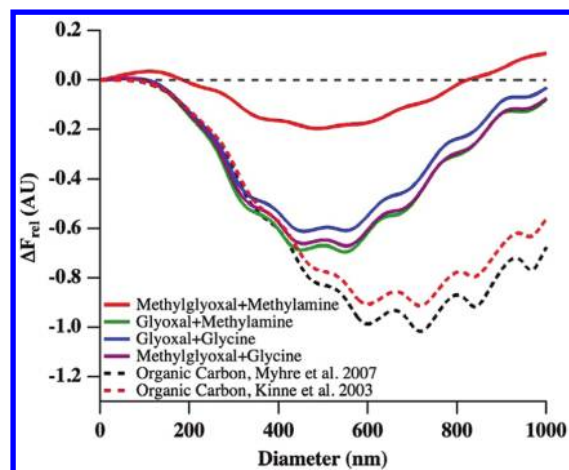


Figure 5. Forcing ratios (in arbitrary units) for the optical constants calculated in this study (solid lines) and the optical constants used for organic aerosol in models (dashed lines) as a function of particle diameter. Values below zero indicate a net cooling effect.

absorption component for organics.⁶ These additional values are shown in Table 1. The model organic aerosols refractive indices have lower n values than those calculated in this study, and also have significantly lower k values. The methylglyoxal-methylamine system from this study causes significantly less cooling than the other systems, and even causes a slight warming at some sizes. At smaller sizes, the other three systems cause similar amounts of cooling as the model organic aerosols. While the indices of refraction measured in this study have nonzero k values, the values of n are higher than those in the models, and at smaller sizes the increased scattering compensates for the increased absorption. As the particle size increases the absorption term becomes more important, and for particles greater than 500 nm, the forcing calculated using constants from models is significantly more negative than the forcing using the constants measured in this study. The particles examined in this study can cause at least 25% less cooling at larger sizes than particles used in modeling, indicating that the modeled cooling effect of organic aerosol on radiative forcing may be too large.

The overall impact of absorbing aerosol particles on direct radiative forcing depends on both the size and abundance of such particles in the atmosphere. If the peak in particle concentration occurs at smaller diameters, then the effect of these particles on climate will be similar to that of nonabsorbing compounds. However, if a significant fraction of the particles are present at larger diameters, then there will be less cooling than predicted by models. While there is little information regarding the concentration and distributions of brown carbon aerosol particles, there is some information about the distributions of HULIS, which has properties similar to brown carbon. Lin et al.³⁷ measured the mass concentration of HULIS as a function of particle size in southern China. HULIS was present at all sizes from 10 nm to 18 μm , and 80% of the HULIS mass was in the droplet mode, indicating that cloud processing may be playing a role in the formation of HULIS. Lin et al. report mass median aerodynamic diameters (MMAD), and assuming that the aerosols have a log-normal distribution, the MMAD can be converted to number median diameters³⁸ ranging between 240 and 430 nm. If the particles examined in this study adopt a similar size distribution to HULIS, then there will be a significant population of particles at

the larger sizes where absorption dominates, thus reducing the cooling effect of OA on radiative forcing. Better characterization of the size distributions of ambient brown carbon particles is required to more accurately model their effects on climate, but it is clear that absorbing organic compounds can affect climate differently than has been previously assumed.

AUTHOR INFORMATION

Corresponding Author

*E-mail Tolbert@colorado.edu.

Present Address

^{||}Department of Chemistry, The Pennsylvania State University, 104 Chemistry Building, University Park, Pennsylvania 16802

Notes

The authors declare no competing financial interest.

ACKNOWLEDGMENTS

This work was supported by the National Aeronautics and Space Administration under Grant No. NNX09AE12G. MAF was supported by the NOAA Climate and Global Change Postdoctoral Fellowship Program administered by the University Corporation for Atmospheric Research. Atomic force microscopy was performed at the University of Colorado Nanomaterials Characterization Facility.

REFERENCES

- (1) Charlson, R. J.; Schwartz, S. E.; Hales, J. M.; Cess, R. D.; Coakley, J. A.; Hansen, J. E.; Hofmann, D. J. Climate forcing by anthropogenic aerosols. *Science* **1992**, *225* (5043), 423–430.
- (2) Chylek, P.; Wong, J. Effect of absorbing aerosols on global radiation budget. *Geophys. Res. Lett.* **1995**, *22* (8), 929–931.
- (3) Zhang, Q.; Jimenez, J. L.; Canagaratna, M. R.; Allan, J. D.; Coe, H.; Ulbrich, I.; Alfarra, M. R.; Takami, A.; Middlebrook, A. M.; Sun, Y. L.; et al. Ubiquity and dominance of oxygenated species in organic aerosol in anthropogenically-influenced Northern Hemisphere mid-latitudes. *Geophys. Res. Lett.* **2007**, *34*, L13801.
- (4) Stelson, A. W. Urban aerosol refractive index prediction by partial molar refraction approach. *Environ. Sci. Technol.* **1990**, *24* (11), 1676–1679.
- (5) Myhre, G.; Bellouin, N.; Berglen, T. F.; Berntsen, T. K.; Boucher, O.; Grini, A.; Isaksen, I. S. A.; Johnsrud, M.; Mishchenko, M. I.; Stordal, F.; Tanrè, D. Comparison of the radiative properties and direct radiative effect of aerosols from a global aerosol model and remote sensing data over ocean. *Tellus* **2007**, *59B* (1), 115–129.
- (6) Kinne, S.; Lohmann, U.; Feichter, J.; Schulz, M.; Timmreck, C.; Ghan, S.; Easter, R.; Chin, M.; Ginoux, P.; Takemura, T.; et al. Monthly averages of aerosol properties: A global comparison among models, satellite data, and AERONET ground data. *J. Geophys. Res.* **2003**, *108*, 4634.
- (7) Andreae, M. O.; Gelencser, A. Black carbon or brown carbon? The nature of light-absorbing carbonaceous aerosols. *Atmos. Chem. Phys.* **2006**, *6*, 3131–3148.
- (8) Yang, M.; Howell, S. G.; Zhuang, J.; Huebert, B. J. Attribution of aerosol light absorption to black carbon, brown carbon, and dust in China—Interpretations of atmospheric measurements during EAST-AIRE. *Atmos. Chem. Phys.* **2009**, *9*, 2035–2050.
- (9) Barnard, J. C.; Volkamer, R.; Kassianov, E. I. Estimation of the mass absorption cross section of the organic carbon component of aerosols in the Mexico City Metropolitan Area. *Atmos. Chem. Phys.* **2008**, *8*, 6665–6679.
- (10) Dinar, E.; Riziq, A. A.; Spindler, C.; Erlick, C.; Kiss, G.; Rudich, Y. The complex refractive index of atmospheric and model humic-like substances (HULIS) retrieved by a cavity ring down aerosol spectrometer (CRD-AS). *Faraday Discuss.* **2008**, *137*, 279–295.
- (11) Hoffer, A.; Gelencsèr, A.; Guyon, P.; Kiss, G.; Schmid, O.; Frank, G. P.; Artaxo, P.; Andreae, M. O. Optical properties of humic-

like substances (HULIS) in biomass-burning aerosols. *Atmos. Chem. Phys.* **2006**, *6*, 3563–3570.

(12) Kirchstetter, T. W.; Novakov, T.; Hobbs, P. V. Evidence that the spectral dependence of light absorption by aerosols is affected by organic carbon. *J. Geophys. Res.* **2004**, *109* (D21), D21208.

(13) Lim, Y. B.; Tan, Y.; Perri, M. J.; Seitzinger, S. P.; Turpin, B. J. Aqueous chemistry and its role in secondary organic aerosol (SOA) formation. *Atmos. Chem. Phys.* **2010**, *10*, 10521–10539.

(14) Ervens, B.; Turpin, B. J.; Weber, R. J. Secondary organic aerosol formation in cloud droplets and aqueous particles (aqSOA): A review of laboratory, field and model studies. *Atmos. Chem. Phys.* **2011**, *11*, 11069–11102.

(15) Nozière, B.; Esteve, W. Organic reactions increasing the absorption index of atmospheric sulfuric acid aerosols. *Geophys. Res. Lett.* **2004**, *32*, L03812.

(16) Nozière, B.; Dziedzic, P.; Córdova, A. Formation of secondary light-absorbing “fulvic-like” oligomers: A common process in aqueous and ionic atmospheric particles? *Geophys. Res. Lett.* **2007**, *34*, L21812.

(17) Bones, D. L.; Henricksen, D. K.; Mang, S. A.; Gonsior, M.; Bateman, A. P.; Nguyen, T.; Cooper, W. J.; Nizkorodov, S. A. Appearance of strong absorbers and fluorophores in limonene-O₃ secondary organic aerosol due to NH₄⁺-mediated chemical aging over long time scales. *J. Geophys. Res.* **2010**, *115*, D05203.

(18) Shapiro, E. L.; Szprengiel, J.; Sareen, N.; Jen, C. N.; Giordana, M. R.; McNeill, V. F. Light-absorbing secondary organic material formed by glyoxal in aqueous aerosol mimics. *Atmos. Chem. Phys.* **2009**, *9*, 2289–2300.

(19) Sareen, N.; Schwier, A. N.; Shapiro, E. L.; Mitroo, D.; McNeill, V. F. Secondary organic material formed by methylglyoxal in aqueous aerosol mimics. *Atmos. Chem. Phys.* **2010**, *10*, 997–1016.

(20) Yu, G.; Bayer, A. R.; Galloway, M. M.; Korshaven, K. J.; Fry, C. G.; Keutsch, F. N. Glyoxal in aqueous ammonium sulfate solutions: Products, kinetics and hydration effects. *Environ. Sci. Technol.* **2011**, *45* (15), 6336–6342.

(21) De Haan, D. O.; Corrigan, A. L.; Smith, K. W.; Stroik, D. R.; Turley, J. J.; Lee, F. E.; Tolbert, M. A.; Jimenez, J. L.; Cordova, K. E.; Ferrell, G. R. Secondary organic aerosol-forming reactions of glyoxal with amino acids. *Environ. Sci. Technol.* **2009a**, *43* (8), 2818–2824.

(22) De Haan, D. O.; Tolbert, M. A.; Jimenez, J. L. Atmospheric condensed-phase reactions of glyoxal with methylamine. *Geophys. Res. Lett.* **2009b**, *36*, L11819.

(23) De Haan, D. O.; Hawkins, L. N.; Kononenko, J. A.; Turley, J. J.; Corrigan, A. L.; Tolbert, M. A.; Jimenez, J. L. Formation of nitrogen-containing oligomers by methylglyoxal and amines in simulated evaporating cloud droplets. *Environ. Sci. Technol.* **2011**, *45* (3), 984–991.

(24) Denkenberger, K. A.; Moffet, R. C.; Holecek, J. C.; Rebotier, T. P.; Prather, K. A. Real-time, single-particle measurements of oligomers in aged ambient aerosol particles. *Environ. Sci. Technol.* **2007**, *41* (15), 5439–5446.

(25) Wang, X.; Gao, S.; Yang, X.; Chen, H.; Chen, J.; Zhuang, G.; Surratt, J. D.; Chan, M. N.; Seinfeld, J. H. Evidence for high molecular weight nitrogen-containing organic salts in urban aerosols. *Environ. Sci. Technol.* **2010**, *44* (12), 4441–4446.

(26) Munger, J. W.; Jacob, D. J.; Daube, B. C.; Horowitz, L. W. Formaldehyde, glyoxal, and methylglyoxal in air and cloudwater at a rural mountain site in central Virginia. *J. Geophys. Res.* **1995**, *100*, 9325–9333.

(27) Zhang, Q.; Anastasio, C. Free and combined amino compounds in atmospheric fine particles (PM_{2.5}) and fog waters from Northern California. *Atmos. Environ.* **2003**, *37*, 2247–2258.

(28) Freedman, M. A.; Hasenkopf, C. A.; Beaver, M. R.; Tolbert, M. A. Optical properties internally mixed aerosol particles composed of dicarboxylic acids and ammonium sulfate. *J. Phys. Chem. A* **2009**, *113* (48), 13584–13592.

(29) Hasenkopf, C. A.; Beaver, M. R.; Trainer, M. G.; DeWitt, H. L.; Freedman, M. A.; Toon, O. B.; McKay, C. P.; Tolbert, M. A. Optical properties of Titan and early Earth haze laboratory analogs in the mid-visible. *Icarus* **2010**, *207* (2), 903–913.

(30) DeCarlo, P. F.; Slowik, J. G.; Worsnop, D. R.; Davidovits, P.; Jimenez, J. L. Particle morphology and density characterization by combined mobility and aerodynamic diameter measurements. Part 1: Theory. *Aerosol. Sci. Tech.* **2004**, *38* (12), 1185–1205.

(31) Wiedensohler, A. An approximation of the bipolar charge-distribution for particles in the sub-micron size range. *J. Aerosol. Sci.* **1988**, *19* (3), 387–389.

(32) Mätzler, C. *IAP Research Report, No. 2002-08* [Online]; Universität Bern: Bern, Switzerland, 2002; http://diogenes.iwt.unibremen.de/vt/laser/wriedt/Mie_Type_Codes/body_mie_type_codes.html (accessed May 2009).

(33) Bohren, C. F.; Huffman, D. R. *Absorption and Scattering of Light by Small Particles*; Wiley-VCH: Weinheim, Germany, 2004.

(34) Abo Riziq, A.; Erlick, C.; Dinar, E.; Rudich, Y. Optical properties of absorbing and non-absorbing aerosols retrieved by cavity ring down (CRD) spectroscopy. *Atmos. Phys. Chem.* **2007**, *7*, 1523–1536.

(35) Davidek, T.; Velišek, J.; Davidek, J.; Pech, P. Glycylglycine-derived 1,3-disubstituted imidazole in nonenzymatic browning reactions. *J. Agric. Food Chem.* **1991**, *39*, 1374–1377.

(36) Graber, E. R.; Rudich, Y. Atmospheric HULIS: How humic-like are they? A comprehensive and critical review. *Atmos. Chem. Phys.* **2006**, *6*, 729–753.

(37) Lin, P.; Huang, X.-F.; He, L.-Y.; Yu, J. Z. Abundance and size distributions of HULIS in ambient aerosols at a rural site in South China. *J. Aerosol Sci.* **2010**, *41* (1), 74–87.

(38) Seinfeld, J. H.; Pandis, S. N. *Atmospheric Chemistry and Physics*, Chapter 8; John Wiley & Sons: Hoboken, NJ, 2006.